Neoclassical calculation of poloidal rotation and poloidal density asymmetries in tokamaks

Weston M. Stacey
Fusion Research Center, Georgia Institute of Technology, Atlanta, Georgia 30332

(Received 9 April 2002; accepted 28 May 2002)

A previous model for the calculation of poloidal velocities and poloidal density asymmetries in the core of a tokamak plasma is refined and extended by the inclusion of terms which are important for the calculation of these quantities in the plasma edge. Agreement of predictions of the model with experiment is demonstrated. The effects of edge pressure gradient, collisionality, neutral density and up–down flux surface asymmetry on the edge poloidal rotation velocities are illustrated by a series of model problem calculations. © *2002 American Institute of Physics.* [DOI: 10.1063/1.1497371]

I. INTRODUCTION

Several years ago, we developed[1] a "first-principles" neoclassical calculation of the poloidal rotation and poloidal density asymmetries over the flux surface in a multi-species tokamak plasma, based on solution of the particle and poloidal momentum balance equations. When toroidal rotation speeds (and densities and temperatures) were taken from experiment, the calculation predicted poloidal rotation speeds and density asymmetries which, when used to evaluate the neoclassical gyroviscous momentum transport rate,[2] led to the prediction of momentum confinement times and central toroidal rotation speeds in agreement with measured values for a number of different tokamaks.[3]

More recently, this calculation of poloidal velocities and density asymmetries,[1] which requires toroidal velocities as input, has been coupled with a neoclassical calculation of the toroidal velocities. The coupling is via a neoclassical gyroviscous model[2] for radial momentum transport, which requires the poloidal velocities and density asymmetries as input. The iterative coupling of these three models provides a self-contained and self-consistent neoclassical calculation of poloidal and toroidal rotation[4] that requires only the external momentum input (and plasma density and temperature) as input. This combined calculation has been successful in predicting toroidal rotation velocities and momentum confinement times in agreement with a wide range of DIII-D experiments[5,6] and in predicting the measured poloidal rotation in the one DIII-D shot for which a comparison has been made to date.

Given this measure of confirmation of the theory and the growing importance of poloidal rotation (e.g., the observation of changes in poloidal rotation at the $L-H$ transition[7–9]), we have undertaken to refine the existing model for the calculation of poloidal rotation and density asymmetries in the plasma core and to extend its applicability to the edge region, where ionization sources, charge-exchange momentum sinks, pressure gradients and up–down asymmetries in both the flux surface geometry and the ionization sources become important. The purpose of this paper is to report this development of a refined and extended calculation of poloidal rotation and density asymmetries over the flux surface in tokamaks and its application to investigate poloidal rotation in tokamak plasmas.

II. CALCULATION MODEL

A. Basic equations

The calculation model is derived from the basic particle balance

$$\nabla\cdot(n_j\mathbf{v}_j)=S_j\,, \tag{1}$$

and momentum balance equations

$$n_j m_j(\mathbf{v}_j\cdot\nabla)\mathbf{v}_j+\nabla\cdot\overleftrightarrow{\boldsymbol{\pi}}_j+\nabla p_j+e_j n_j\nabla\Phi+n_j e_j\mathbf{v}_j\times\mathbf{B}$$
$$=\boldsymbol{M}_j+\boldsymbol{R}_j-m_j S_j\mathbf{v}_j\,, \tag{2}$$

where n_j, $\mathbf{v}_j$, m_j, e_j, p_j, and $\boldsymbol{\pi}_j$ are the particle density, velocity, mass, pressure, and viscosity tensor of ion species "j." $\boldsymbol{R}_j$ and $\boldsymbol{M}_j$ are the interspecies collisional momentum exchange and the external momentum source or sink for species "j," and S_j is the particle source for species "j."

B. Coordinate system and flux surface geometry

We use a right hand $(r\text{-}\theta\text{-}\phi)$ toroidal coordinate system, where r is the minor radius, θ is the poloidal angle measured from the outboard midplane, and ϕ is the toroidal angle. The positive ϕ-direction is defined to be the direction of the plasma current, so that B_θ is always positive. When the toroidal field is parallel to the plasma current, $B_\phi>0$ and when the toroidal field is opposite to the plasma current, $B_\phi<0$. When the toroidal component of the beam injection direction is parallel to the plasma current, M_ϕ and v_ϕ are positive, and when it is opposite to the current direction they are negative.

Noncircular plasma geometries are represented by equivalent circular geometries; e.g., a plasma with minor radius "a" and elongation κ is represented by a circle with an equivalent minor radius $a_{\rm eq}=a((1+\kappa^2)/2)^{1/2}$ that conserves surface area and an equivalent radial coordinate $r_{\rm eq}=r((1+\kappa^2)/2)^{1/2}$.

The in–out asymmetry introduced by the toroidal geometry is represented by writing $R=R_0(1+\epsilon\cos\theta)$ and B_θ

$=B_\theta^o(1+\epsilon\cos\theta)$. We represent the up–down asymmetry in the poloidal magnetic field associated with a single null divertor by writing

$$B_\theta(r,\theta)=\begin{cases}\dfrac{B_\theta^o(r)}{1+\epsilon\cos\theta+\xi\sin\theta H_o^\pi} & \text{USN}\\ \dfrac{B_\theta^o(r)}{1+\epsilon\cos\theta-\xi\sin\theta H_\pi^{2\pi}} & \text{LSN}\end{cases}, \tag{3}$$

where USN and LSN refer to ''upper single null'' and ''lower single null,'' respectively, and H is the Heaviside function. $H_0^\pi=1$ in the interval $0\leqslant\theta\leqslant\pi$ and vanishes in the interval $\pi\leqslant\theta\leqslant2\pi$ to approximate the effect of an upper single null divertor in weakening the poloidal field in the upper part of the plasma. Similary, $H_\pi^{2\pi}=1$ for $\pi\leqslant\theta\leqslant2\pi$ and vanishes for $0\leqslant\theta\leqslant\pi$ to represent the effect of a lower single null divertor in weakening the poloidal field in the lower part of the plasma.

C. Ordering

We consider an ordering that is appropriate for a strongly rotating plasma ($v_\phi\approx v_{\rm th}$, $E\approx B_\theta$) with sharp gradients ($L\equiv((-1/p)\partial p/\partial r)^{-1}\approx\rho_\theta\equiv mv_{\rm th}/eB_\theta$) and make the usual tokamak assumptions about the ratio of the poloidal and toroidal magnetic fields ($\beta\equiv B_\theta/B_\phi\ll1$) and the magnitude of the minor to major radii ($\epsilon\equiv r/R<1$). We further restrict the up-down asymmetry factor to the range $0\leqslant\xi<1$.

D. Constitutive relations

We use the simple Lorentz model for the collisional momentum exchange

$$\boldsymbol{R}_j=-n_jm_j\sum_{k\neq j}\nu_{jk}(\mathbf{v}_j-\mathbf{v}_k). \tag{4}$$

We use the neoclassical parallel viscosity tensor obtained by extending the classical rate-of-strain tensor formalism to toroidal geometry[2] and use a neoclassical parallel viscosity coefficient[10] that takes banana-plateau collisionality effects into account

$$\eta_{oj}=\frac{n_jm_jv_{{\rm th}j}qR\epsilon^{-3/2}\nu_{jj}^*}{(1+\epsilon^{-3/2}\nu_{jj}^*)(1+\nu_{jj}^*)}\equiv n_jm_jv_{{\rm th}j}qRf_j(\nu_{jj}^*), \tag{5}$$

where $q=|rB_\phi/RB_\theta|=\epsilon/|\beta|$ is the safety factor and the normalized collision frequency is $\nu_{jk}^*=\nu_{jk}qR/v_{{\rm th}j}$. The poloidal component of the divergence of the parallel viscosity tensor, which is the only component that we will need, can be written[2]

$$\hat{n}_\theta\cdot\nabla\cdot\boldsymbol{\pi}_j=\eta_{oj}\left(\frac{1}{2}A_{oj}\right)\left\{\frac{1}{r}\frac{\partial\ell n(\eta_{oj}A_{oj})}{\partial\theta}-\frac{3\sin\theta}{R}\right\}, \tag{6}$$

where

$$\frac{1}{2}A_{oj}=\left\{-\frac{1}{3}\frac{1}{r}\frac{\partial v_{\theta j}}{\partial\theta}+v_{\theta j}\left(\frac{1}{R}\frac{1}{r}\frac{\partial R}{\partial\theta}+\frac{1}{3}\frac{1}{B_\theta}\frac{1}{r}\frac{\partial B_\theta}{\partial\theta}\right)+\left(\frac{B_\theta}{B_\phi}\right)\frac{R}{r}\frac{\partial(v_{\phi j}/R)}{\partial\theta}\right\}. \tag{7}$$

E. Form of the toroidal velocity

The radial component of the momentum balance equation, Eq. (2), yields a relationship among the toroidal velocity and the density, poloidal velocity, electrostatic potential, and magnetic field

$$v_{\phi j}(r,\theta)=\left(\frac{B_\phi}{B_\theta}\right)v_{\theta j}(r,\theta)-\Phi'(r,\theta)-P_j'(r,\theta), \tag{8}$$

where

$$\Phi'\equiv\frac{1}{B_\theta}\frac{\partial\Phi}{\partial r},\qquad P_j'\equiv\frac{1}{B_\theta n_je_j}\frac{\partial p_j}{\partial r}. \tag{9}$$

In the subsequent development, we will use Eq. (8) to represent the poloidal dependence of the toroidal velocity in terms of the poloidal dependence of the other quantities appearing in that equation, then use the flux surface average of this equation

$$\overline{\Phi}'(r)\equiv\frac{B_\phi^o}{B_\theta^o}\overline{v}_{\theta j}(r)-\overline{v}_{\phi j}(r)-\overline{P}_j'(r), \tag{10}$$

to replace $\overline{\Phi}'$ with $\overline{v}_{\phi j}$, $\overline{v}_{\theta j}$ and pressure gradient terms in the final result.

F. Form of the poloidal velocity

Taking the flux surface average (denoted by $\langle\ \rangle$) of Eq. (1), noting that the lowest order particle fluxes are within the flux surface and assuming axisymmetry yields $\langle\nabla\cdot n_j\mathbf{v}_j\rangle=\langle S_j\rangle\equiv\overline{S}_j$, which may be subtracted from Eq. (1) to obtain

$$\frac{1}{r}\frac{\partial}{\partial\theta}((1+\epsilon\cos\theta)n_jv_{\theta j})=(1+\epsilon\cos\theta)(S_j-\overline{S}_j), \tag{11}$$

in toroidal geometry. This equation can be integrated to obtain a ''surface function of integration,'' $K_j(\theta)$, and a particular solution arising from the inhomogeneous particle source term. K_j can be determined by flux surface averaging the resulting equation and setting it equal to the average value over the flux surface of the poloidal velocity, $\overline{v}_{\theta j}$

$$v_{\theta j}(r,\theta)=\frac{\overline{n_j}(r)\overline{v}_{\theta j}(r)+r\int_o^\theta(1+\epsilon\cos\theta')[S_j(r,\theta')-\overline{S}_j(r)]d\theta'}{1+\epsilon\cos\theta}. \tag{12}$$

Thus, the θ-dependence of the poloidal velocity depends on the θ-dependence of the density and ionization source and on the toroidal geometry metric $(1+\epsilon\cos\theta)$.

We will develop equations for the determination of the $\overline{v}_{\theta j}$ in a later section.

G. Form of the inertial term

Taking into account that the particle fluxes in the flux surface are much greater than the particle flux across the flux

surface to drop v_r terms, we can write the poloidal component of the inertial term, which is the only one that we will need, as

$$\hat{n}_\theta \cdot (\mathbf{v}_j \cdot \nabla)\mathbf{v}_j \simeq \frac{1}{2}\frac{1}{r}\frac{\partial v_{\theta j}^2}{\partial \theta} + \frac{v_{\phi j}^2}{R}\sin\theta. \tag{13}$$

H. Representation of poloidal density asymmetry

We represent the poloidal asymmetry over the flux surface of the particle density by a low order Fourier series expansion

$$n_j(r,\theta) = (1 + n_j^c(r)\cos\theta + n_j^s(r)\sin\theta + \cdots). \tag{14}$$

We will develop equations to solve for the $n_j^{c/s}$.

We expect that a low-order Fourier expansion will be adequate because the flux surface geometry and the neutral ionization source (see subsequent discussion) both have a low-order Fourier asymmetry ($\sin\theta$ and $\cos\theta$).

I. Ionization and neutral beam ion sources

The source of ions in the edge plasma is due to the ionization of recycling and fueling neutrals. Although fueling neutrals are introduced into the plasma chamber at poloidally localized sites, by the time they have diffused inward across the separatrix into the edge plasma they will have spread poloidally. Similarly, recycling neutrals in diverted plasmas will originate at the divertor plate, which constitutes a source that is highly localized at the top or bottom of the plasma, but this source will spread poloidally by the time the neutrals have diffused across the separatrix into the edge plasma. Thus, we represent the distribution of such neutrals in the edge plasma as a low-order Fourier expansion

$$n_{oj}(r,\theta) = \overline{n}_{oj}(r)(1 + n_{oj}^c(r)\cos\theta + n_{oj}^s(r)\sin\theta + \cdots), \tag{15}$$

where the coefficients must be determined by evaluating the Fourier components of the calculated or measured neutral density, $n_o(r,\theta)$

$$\begin{aligned} n_o^c(r) &= \int_o^{2\pi} n_o(r,\theta)\cos\theta d\theta/\overline{n}_o\pi, \\ n_o^s(r) &= \int_o^{2\pi} n_o(r,\theta)\sin\theta d\theta/\overline{n}_o\pi. \end{aligned} \tag{16}$$

Fast ions formed by the ionization or charge-exchange of neutral beams will be initially created along the path of the beam. However, by the time these fast ions have slowed down to become a source of thermal ions they will have been spread over the flux surface. For example, a beam injected horizontally at the outboard midplane will produce a source of fast ions localized poloidally at $\theta = 0$, but by the time these ions slow down to thermal their poloidal asymmetry can be represented by $\cos\theta$.

Thus, we represent the ionization source for species "j" as

$$\begin{aligned} S_j(r,\theta) &= n_j(r,\theta) n_{oj}(r,\theta)\langle\sigma v\rangle_{\text{ion}} \\ &= \overline{n}_j(r)(1 + n_j^s\sin\theta + n_j^c\cos\theta + \cdots)\overline{n}_{oj}(r) \\ &\quad \times (1 + n_{oj}^s\sin\theta + n_{oj}^c\cos\theta + \cdots)\langle\sigma v\rangle_{\text{ion}} \\ &\equiv \overline{n}_j(r)\,\nu_{\text{ion}}(r)(1 + (n_j^s + n_{oj}^s)\sin\theta \\ &\quad + (n_j^c + n_{oj}^c)\cos\theta + \cdots). \end{aligned} \tag{17}$$

We note that the accuracy of a low-order Fourier representation of the poloidal distribution of the ion source arising from pellet fueling is questionable, and it may be necessary to go to a higher order representation.

J. Asymmetric radial particle flux

We allow for the possibility of a poloidally asymmetric radial particle flux by writing

$$v_r(r,\theta) = \overline{v}_r(r)(1 + v_r^s\sin\theta + v_r^c\cos\theta + \cdots), \tag{18}$$

where the Fourier coefficients $v_r^{c/s}$ must be determined from other calculations.

K. Electrostatic potential representation

The poloidal dependence of the electrostatic potential is represented as

$$\Phi(r,\theta) = \overline{\Phi}(r)(1 + \Phi^s(r)\sin\theta + \Phi^c(r)\cos\theta + \cdots), \tag{19}$$

and the poloidal component of the electron momentum balance is used to relate the Fourier coefficients for the electrostatic potential to the Fourier coefficients of the ion densities

$$\left(\frac{e\overline{\Phi}}{T_e}\right)\Phi^{c/s} = n_e^{c/s} = \sum_j^{\text{ions}} z_j \frac{\overline{n_j}}{\overline{n_e}} n_j^{c/s}. \tag{20}$$

L. Moments equations

We develop equations for determining the $\overline{v}_{\theta j}$ and the $n_j^{c/s}$ by taking moments of the poloidal component of Eq. (2) weighted by 1, $\cos\theta$, $\sin\theta$,... and flux surface averaging. To simplify the subsequent evaluation of the moments equations, we divide Eq. (2) by $n_j m_j(1 + \epsilon\cos\theta)$ before taking the flux surface average

$$\left\langle \frac{(\hat{n}_\theta \cdot \text{Eq.}(2))X}{n_j m_j(1 + \epsilon\cos\theta)} \right\rangle, \quad X = 1,\ \sin\theta,\ \cos\theta, \ldots. \tag{21}$$

After considerable algebraic reduction, retaining terms through quadratic in the small quantities $(\epsilon, \xi, n_j^{c/s}, n_{oj}^{c/s}, \Phi^{c/s})$, these equations can be written

$X=1$

$$\hat{v}_{\theta j}\left[-q^2\hat{v}_{\phi j}\frac{\beta}{|\beta|}\{\tilde{\Phi}^s+\tilde{n}_j^s\}-q^2 f_j\left\{\frac{3}{2}+\frac{3}{2}\tilde{n}_j^c+\frac{1}{3}(\tilde{n}_j^s)^2+\frac{1}{3}(\tilde{n}_j^c)^2+\frac{1}{2}\tilde{n}_j^s\tilde{\Phi}^s+\frac{1}{2}(\tilde{n}_j^c+3)\tilde{\Phi}^c-\frac{1}{6}\tilde{\xi}\tilde{n}_j^s\right\}+\sum_{k\neq j}\nu_{jk}^*+\overline{\nu}_{\mathrm{ion}j}^*\right]$$
$$=-\frac{\hat{v}_{rj}}{\beta}+\hat{M}_{\theta j}+\sum_{k\neq j}\nu_{jk}^*\sqrt{\frac{m_j}{m_k}}\hat{v}_{\theta k}-q^2\hat{v}_{\phi j}\left[\hat{v}_{\phi j}\left\{\tilde{\Phi}^s\pm\frac{1}{2}\tilde{\xi}\right\}+\hat{P}_j'\{\tilde{\Phi}^s\}-\frac{\beta}{|\beta|}\overline{\nu}_{\mathrm{ion}j}^*\{\tilde{n}_j^c+\tilde{n}_{oj}^c\}\right]$$
$$-q^2 f_j\left[\frac{\beta}{|\beta|}(\hat{v}_{\phi j}+\hat{P}_j')\left\{\frac{1}{2}\tilde{n}_j^s\tilde{\Phi}^s+\frac{1}{2}(\tilde{n}_j^c+3)\tilde{\Phi}^c\right\}\pm\hat{v}_{\phi j}\left\{\frac{1}{4}\tilde{n}_j^s\tilde{\xi}\right\}-\overline{\nu}_{\mathrm{ion}j}^*\left\{\tilde{n}_j^s+\tilde{n}_{oj}^s+\frac{1}{3}\tilde{n}_j^c\tilde{n}_{oj}^s-\frac{1}{3}\tilde{n}_j^s\tilde{n}_{oj}^c\right\}\right], \tag{22}$$

$X=\sin\theta$

$$\tilde{n}_j^s\left[\left(\frac{2}{3}f_j\left(1-\frac{4}{3}\frac{\tilde{\xi}\epsilon}{\pi}\right)-\beta^2\sum_{k\neq j}\nu_{jk}^*\right)\hat{v}_{\theta j}-\beta^2\hat{M}_{\theta j}-\frac{2}{3}\frac{\beta}{|\beta|}f_j\hat{v}_{\phi j}\frac{\tilde{\xi}\epsilon}{\pi}\right]-\tilde{n}_j^c\left[\frac{1}{2}+\overline{\nu}_{\mathrm{ion}j}^*\left(\frac{2}{3}f_j-\beta^2\left(\sum_{k\neq j}\nu_{jk}^*+\overline{\nu}_{\mathrm{ion}j}^*\right)\right)\right]$$
$$=-\hat{v}_{\phi j}^2\left(1+\frac{8\epsilon\tilde{\xi}}{3\pi}\right)+f_j\left[\frac{\beta}{|\beta|}(\hat{v}_{\phi j}+\hat{P}_j')\tilde{\Phi}^s-\frac{2}{3}\overline{\nu}_{\mathrm{ion}j}^*\tilde{n}_{oj}^c\right]$$
$$+\frac{1}{2}\hat{\Phi}_j\tilde{\Phi}^c-\beta\hat{v}_{rj}\tilde{v}_{rj}^s-\beta^2\sum_{k\neq j}\nu_{jk}^*\tilde{n}_k^s\hat{v}_{\theta k}\sqrt{\frac{m_j}{m_k}}+\beta^2\hat{M}_{\theta j}\tilde{M}_{\theta j}^s+\overline{\nu}_{\mathrm{ion}j}^*\beta^2$$
$$\times\left[\sum_{k\neq j}\nu_{jk}^*\sqrt{\frac{m_j}{m_k}}(\tilde{n}_k^c+\tilde{n}_{ok}^c)-2\tilde{n}_{oj}^s\hat{v}_{\theta j}-\overline{\nu}_{\mathrm{ion}j}^*\tilde{n}_{oj}^c\right], \tag{23}$$

$X=\cos\theta$

$$\tilde{n}_j^c\left[\left(\frac{2}{3}f_j\left(1+\frac{4}{3}\frac{\tilde{\xi}\epsilon}{\pi}\right)-\beta^2\sum_{k\neq j}\nu_{jk}^*\right)\hat{v}_{\theta j}+\beta^2\hat{M}_{\theta j}-\frac{2}{3}\frac{\beta}{|\beta|}f_j\hat{v}_{\phi j}\frac{\tilde{\xi}\epsilon}{\pi}\right]+\tilde{n}_j^s\left[\frac{1}{2}+\overline{\nu}_{\mathrm{ion}j}^*\left(\frac{2}{3}f_j-\beta^2\left(\sum_{k\neq j}\nu_{jk}^*+\overline{\nu}_{\mathrm{ion}j}^*\right)\right)\right]$$
$$=-f_j\left[\hat{v}_{\theta j}\left\{1+\tilde{\Phi}^c+\frac{8}{3}\frac{\tilde{\xi}\epsilon}{\pi}\right\}+\frac{2}{3}\overline{\nu}_{\mathrm{ion}j}^*\tilde{n}_{oj}^s\right]-f_j\left[\frac{\beta}{|\beta|}\left\{(\hat{v}_{\phi j}+\hat{P}_j')\tilde{\Phi}^c+\hat{v}_{\phi j}\tilde{\xi}\left(\mp\frac{1}{2}+\frac{2\epsilon}{\pi}\right)\right\}\right]$$
$$-\frac{1}{2}\hat{\Phi}_j\tilde{\Phi}^s+\beta\hat{v}_{rj}(1-\tilde{v}_{rj}^c)+\beta^2\sum_{k\neq j}\nu_{jk}^*\left(\hat{v}_{\theta j}-\sqrt{\frac{m_j}{m_k}}(1+\tilde{n}_k^c)\hat{v}_{\theta k}\right)+\beta^2\hat{M}_{\theta j}\tilde{M}_{\theta j}^c$$
$$-\overline{\nu}_{\mathrm{ion}j}^*\beta^2\left[\sum_{k\neq j}\nu_{jk}^*\sqrt{\frac{m_j}{m_k}}(\tilde{n}_k^s+\tilde{n}_{ok}^s)+(2\tilde{n}_{oj}^c-1)\hat{v}_{\theta j}-\overline{\nu}_{\mathrm{ion}j}^*\tilde{n}_{oj}^s\right]. \tag{24}$$

The terms in Eqs. (22)–(24) are

$$\hat{v}_{\theta j}\equiv\frac{\overline{v}_{\theta j}}{|\beta|v_{\mathrm{th}j}},\quad \hat{v}_{\phi j}\equiv\frac{\overline{v}_{\phi j}}{v_{\mathrm{th}j}},$$

$$\hat{v}_{rj}\equiv\frac{\overline{v}_{rj}}{\left(\frac{mv_{\mathrm{th}j}}{e_jB_\theta^o}\right)|\beta|\left(\frac{v_{\mathrm{th}j}}{qR}\right)},\quad \beta\equiv\frac{B_\theta}{B_\phi},$$

$$\tilde{n}_j^{c/s}\equiv\frac{n_j^{c/s}}{\epsilon},\quad \tilde{\Phi}^{c/s}\equiv\frac{\Phi^{c/s}}{\epsilon},\quad \tilde{n}_{oj}^{c/s}=\frac{n_{oj}^{c/s}}{\epsilon},$$

$$\tilde{\xi}\equiv\frac{\xi}{\epsilon},\quad \tilde{M}_{\theta j}^{c/s}\equiv\frac{M_{\theta j}^{c/s}}{\epsilon}, \tag{25}$$

$$\tilde{v}_{rj}^{c/s}\equiv\frac{v_{rj}^{c/s}}{\epsilon},\quad \nu_{jk}^*\equiv\frac{\nu_{jk}}{\left(\frac{v_{\mathrm{th}j}}{qR}\right)},\quad \overline{\nu}_{\mathrm{ion}j}^*\equiv\frac{\overline{\nu}_{\mathrm{ion}j}}{\left(\frac{v_{\mathrm{th}j}}{qR}\right)},$$

$$\hat{M}_{\theta j}\equiv\frac{\overline{M}_{\theta j}}{\overline{n}_jm_j\left(\frac{v_{\mathrm{th}_j}^2}{q^R}\right)|\beta|},$$

$$\hat{P}_j'=\frac{1}{B_\theta^o\overline{n}_je_jv_{\mathrm{th}j}}\frac{\partial\overline{p}_j}{\partial r},\quad \hat{\Phi}_j\equiv\frac{e_j\overline{\Phi}}{\frac{1}{2}m_jv_{\mathrm{th}j}^2}=\frac{e_j\overline{\Phi}}{T_j}.$$

A set of Eqs. (22)–(24) obtains for each ion species in the plasma. These equations are explicitly coupled among ion species through the collisional momentum exchange (ν_{jk}^* terms) and through the electrostatic potential, as indicated by Eq. (20). The upper symbol ($\pm$) is taken for USN divertor configurations, and the lower symbol for LSN, in the above equations.

M. Discussion

Equations (22) determine the average poloidal velocities, $\overline{v}_{\theta j}$. The terms on the right may be regarded as driving the poloidal velocity. We can trace through the effect of these terms on the direction of the poloidal velocity, assuming for the moment that the term in square brackets on the left is positive. An outward (positive) radial particle flux drives a negative poloidal rotation. A positive/negative poloidal external momentum source drives a positive/negative poloidal rotation. The collisional momentum exchange with other species drives a poloidal rotation in the direction of the poloidal rotation of the other species. The inertial forces and viscous forces can drive positive or negative poloidal rotation, depending on direction of the beam injection and the toroidal magnetic field relative to the direction of the plasma current, the poloidal location of fueling sources, and the sign of the density Fourier coefficients determined from Eqs. (23) and (24). If the term in square brackets on the left is negative, the directions of the poloidal velocity would be just the opposite. The contribution of collisional effects to the term on the left are positive, and the contribution of inertial and viscous effects can be positive or negative, depending on the factors discussed just above.

Equations (23) and (24) determine the density Fourier coefficients, $n_j^{c/s}$. Other than noting that they depend on the mean poloidal velocities determined from Eqs. (22), on the $n_k^{c/s}$ for other ion species, and on the same factors discussed in the above paragraph, it is difficult to gain any physical insight from their examination.

The effects of the new physics (relative to Ref. 1) that has been added can be identified from the symbols $\nu^*_{\mathrm{ion}j}$ (particle sources), $M_{\theta j}$ (external poloidal momentum sources or sinks), P_j' (pressure gradients), and ξ (up–down flux surface asymmetry). When these new effects are suppressed, Eqs. (22)–(24) reduce to the corresponding equations in Ref. 1, except for a couple of sign and subscript typos in Ref. 1 and some additional terms arising from a better representation of the poloidal dependence of v_ϕ in this paper. The effect of B_ϕ being parallel ($\beta>0$) or opposite ($\beta<0$) to the plasma current is explicitly represented in Eqs. (22)–(24).

N. Toroidal rotation calculation

In order to calculate the toroidal rotation in this paper, we use a volume-integrated momentum balance model

$$\Gamma_\phi = \frac{(2\pi R)\int_o^a \langle R\Sigma_j^{\mathrm{ions}} n_j m_j v_\phi\rangle 2\pi r dr}{\tau_\phi^{\mathrm{th}}}, \tag{26}$$

and the assumption of a common toroidal rotation for all species. We have previously found this simple model to yield results in good agreement with experiment.[5,6] Here, Γ_ϕ is the toroidal torque input (e.g., from neutral beam injection), and

$$\tau_{\phi j}^{\mathrm{th}} \equiv \frac{\Sigma_j^{\mathrm{ions}}\int_o^a \langle R n_j m_j v_\phi\rangle r dr}{\Sigma_j^{\mathrm{ions}}\int_o^a \langle R\hat{n}_\phi\cdot\nabla\cdot\overleftrightarrow{\pi}_j\rangle r dr}, \tag{27}$$

is the toroidal momentum confinement time.

The neoclassical gyroviscous theory[2] is used to calculate the toroidal component of the divergence of the anisotropic stress tensor

$$\langle R\hat{n}_\phi\cdot\nabla\cdot\overleftrightarrow{\pi}_j\rangle = \frac{1}{2}\tilde{\theta}_j G_j \frac{\overline{n}_j m_j T_j}{e_j B_\phi}\frac{\overline{v}_\phi}{R}, \tag{28}$$

where

$$\begin{aligned}\tilde{\theta}_j &\equiv (4+\tilde{n}_j^c)\tilde{v}_{\phi j}^s + \tilde{n}_j^s(1-\tilde{v}_{\phi j}^c)\\ &= (4+\tilde{n}_j^c)[-\hat{v}_{\theta j}\hat{v}_{\phi j}^{-1}(\tilde{\Phi}+\tilde{n}_j^s)+\tilde{\Phi}^s]\\ &\quad + \tilde{n}_j^s[\hat{v}_{\theta j}\hat{v}_{\phi j}^{-1}(2+\tilde{\Phi}^c+\tilde{n}_j^c)-\tilde{\Phi}^c],\end{aligned} \tag{29}$$

$$G_j(r) \equiv -\frac{r}{\eta_{4j}v_\phi}\frac{\partial(\eta_{4j}\overline{v}_\phi)}{\partial r}, \tag{30}$$

and $\overline{\eta}_{4j} = \overline{n}_j m_j T_j / e_j B_\phi^o$.

If $\overline{v}_\phi$ is written as the product of a known (from experiment or assumed) radial profile function and an amplitude factor, $v_{\phi 0}$, and the poloidal velocities and density asymmetries are calculated as discussed in the previous sections, then the above equations can be solved for $v_{\phi 0}$, and $\overline{v}_\phi(r)$ can be constructed by multiplying the known profile function by the calculated $v_{\phi 0}$.

III. ROTATION IN THE CORE PLASMA

A. Comparison with experiment

The above calculation model was applied to calculate the poloidal and toroidal rotation in the core of a L-mode DIII-D shot (#98777 @ 1600 ms) with 4.5 MW co-injected neutral beam power and a principal carbon impurity concentration of 1.1%. The poloidal rotation calculation was made for carbon at $r/a=1/2$ where the up–down asymmetry and the radial pressure gradient were negligible ($\xi\approx 0$, $P_j'\approx 0$) and the radial particle fluxes were small ($v_r\approx 0$), and for horizontal beam injection for which the poloidal beam momentum input was zero ($M_{\theta j}=0$). The calculated ionization source ($v^*_{\mathrm{ion}j}$) due to beam injection was included but was negligible. The results are compared with the measured carbon rotation and experimental quantities constructed therefrom in Table I. Results of a previous calculation using the original poloidal rotation calculation model and the same toroidal rotation calculation are also given in the last column of Table I. Taking into account the numerical approximations (see Ref. 6) and that the uncertainty in the measured poloidal velocity is of order unity,[11] the calculated values are in good agreement with the measure values. Comparing the last two columns of calculated results, it is clear that the refinements and corrections to the calculation model do not make a significant difference in the calculated results for the rotation in the plasma core under the conditions described above.

B. Directionality effects

However, the refinements to the calculation model now allow an unambiguous calculation of the effect of the relative directions of the toroidal field, the plasma current and the neutral beam injection. In shot #98777, the plasma current and the beam injection were in the (positive) counterclock-

TABLE I. Comparison of calculated and measured quantities related to rotation in DIII-D shot #98777 at 1600 ms. ($R=1.7$ m, $a=0.6$ m, $\kappa=1.7$, $B_\phi=-1.6$ T, $I=1.2$ MA, $P_{\rm nbi}=4.5$ MW.)

Quantity	Experiment	Calculated	Calculated (Ref. 6)
$\overline{v_\theta}@r/a=1/2$ (m/s)	-1.7×10^3	-0.7×10^3	-1.9×10^3
$\overline{v_\phi}@r=0$ (m/s)	1.5×10^5	1.38×10^5	1.52×10^5
$E_r@r/a=1/2$ (V/m)	2.3×10^4	2.1×10^4	
τ_ϕ (ms)	73	83	80

wise direction looking down on the tokamak, and the toroidal field was in the (negative) clockwise direction. To investigate directionality effects, we made two other calculations. In one, the current, toroidal field and beam injection were all in the (positive) counterclockwise direction, and in the other the current and the toroidal field were in the (positive) counterclockwise direction but the beam injection was in the (negative) clockwise direction. We note that it is whether the various components are parallel or anti-parallel, not whether they are clockwise or counterclockwise, that matters in the formalism.

The calculated results for these different directionalities are compared in Table II, where $+/-$ indicates parallel/anti-parallel to the plasma current. The calculated rotation velocities (poloidal and toroidal) are quite different when the beam injection is parallel or anti-parallel to the current. This difference arose from a difference in the sin component of the density asymmetry for beam injection parallel and anti-parallel to the plasma current.

C. Collisionality effects

Collisionality enters the calculation of poloidal velocities and density asymmetries through the friction terms (ν_{jk}^*) and the viscosity terms ($f_j[\nu_{jk}^*]$) in Eqs. (22)–(24). The friction terms tend to force the poloidal velocities of all species to take on the same value, as may be seen in Eq. (22). On the other hand, the viscosity terms tend to drive the poloidal velocities of the two species (in a two species model) to be of opposite sign, a result which is not obvious from Eq. (22) but which is found explicitly in early models (e.g., Ref. 10) in which the poloidal velocity was calculated from $\langle B\cdot\nabla\cdot\pi\rangle=0$. Thus, the relationship between the poloidal velocities of the main ion and impurity species can be of the same or opposite signs, depending on the relative importance of the poloidal friction and viscous forces, both of which depend on collisionality. The viscosity function f_j defined by Eq. (5) is plotted against ν_{jj}^* in Fig. 1.

In order to investigate the effect of collisionality, we used the same parameters as discussed above for DIII-D shot #98777 at 1600 ms, but varied the temperature to alter collisionality without altering the plasma mass (see Table III). The deuterium and carbon poloidal rotation velocities are identical at the highest collisionality considered but vary by almost a factor of 2 at the lowest collisionality, and are of the same sign over the entire range of collisionality. This result is consistent with the result found previously in Ref. 12. The variation of the magnitude of the poloidal velocities and of the pobidal density asymmetries with collisionality causes a large variation in the momentum confinement time and central toroidal rotation velocity calculated from Eqs. (26)–(29). In general, momentum confinement is predicted to improve with decreasing collisionality.

IV. ROTATION IN THE EDGE PLASMA

In the edge plasma the pressure gradient (P_j'), the ionization source ($\nu_{{\rm ion}j}^*$), the charge-exchange momentum sink ($M_{\theta j}$) and (in the case of single null divertor configurations) the up–down asymmetry (ξ) terms that were neglected in the core plasma calculations can become important. We use the same DIII-D model parameters as above, and fix the edge toroidal rotation velocity at the measured value of 1.75×10^4 m/s, to investigate the effect of these terms on the calculation of poloidal rotation velocities in the plasma edge.

A. Effect of edge pressure gradient and collisionality

We calculated the poloidal rotation velocities and density asymmetries for the deuterium main ions and the carbon impurity ions for edge temperature and density gradient scale lengths over the range $1\leqslant L_n=L_T\leqslant10$ cm. We carried out the calculation for the measured edge density of 0.75×10^{19} m^3 and temperature of 100 eV, corresponding to collisionalities ($\nu_D^*=0.14$, $\nu_{\rm carb}^*=1.78$), for a lower temperature corresponding to collisionalities ($\nu_D^*=0.51$, $\nu_{\rm carb}^*=6.57$), and for a higher temperature corresponding to collisionalities

TABLE II. Comparison of calculated rotation for different directions of current, toroidal field and beam injection in a model problem with the parameters of DIII-D shot #98777 at 1600 ms. ($R=1.7$ m, $a=0.6$ m, $\kappa=1.7$, $|B_\phi|=1.6$ T, $I=1.2$ MA, $P_{\rm nbi}=4.5$ MW.)

B_ϕ	$P_{\rm nbi}$	$v_{\phi0}$ (m/s)	$v_{\theta D}$ (m/s)[a]	$v_{\theta{\rm carb}}$ (m/s)[a]	E_r (V/m)[a]	τ_ϕ (s)
$-$	$+$	1.38×10^5	-6.8×10^2	-7.4×10^2	2.1×10^4	80
$+$	$+$	1.27×10^5	7.4×10^2	8.2×10^2	1.9×10^4	76
$+$	$-$	6.20×10^4	2.2×10^3	5.3×10^2	-1.3×10^4	37

[a]At $r/a=1/2$.

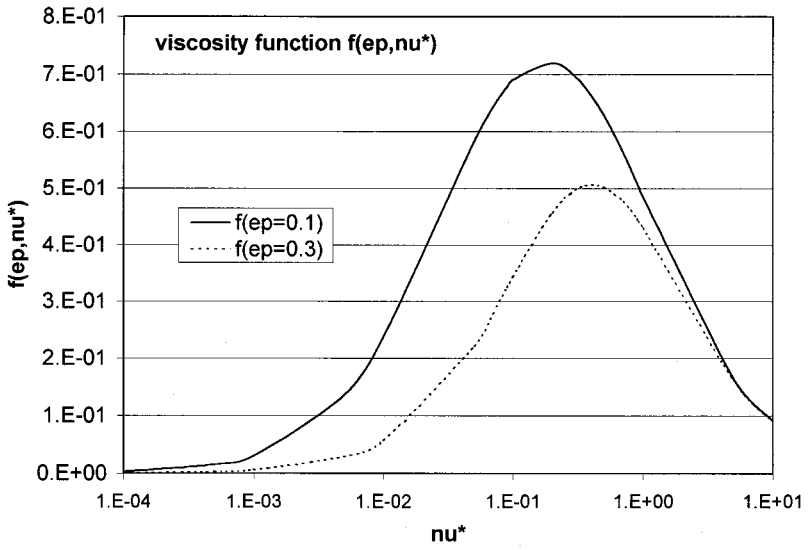

FIG. 1. The viscosity function $f_j(\nu_{jk}^*, \epsilon)$.

($\nu_D^*=0.036$, $\nu_{\text{carb}}^*=0.48$). These three collisionalities are referred to below as "medium," "high," and "low," respectively.

The calculated "ion" (deuterium) and "impurity" (carbon) edge poloidal rotation velocities are plotted versus edge gradient scale length in Fig. 2. At high collisionality (circle), the deuterium and carbon poloidal rotation velocities are essentially identical and vary from slightly positive with weak gradients to significantly negative as the edge gradients increase (gradient scale lengths decrease). For the medium and low collisionality cases, the deuterium and carbon rotation velocities are of opposite sign and increase in magnitude as the gradient scale lengths decrease. Of particular note is the very strong increase in the positive carbon rotation with decreasing gradient scale length for the medium case, for which $\nu_{\text{carb}}^*=1.78$ falls near the peak of the viscosity function f_j plotted in Fig. 1. This strong increase in poloidal rotation velocity with steepening pressure gradient is consistent with the results of Ref. 12.

B. Effect of edge neutral density

The flux of fueling and recycling neutral atoms that penetrate into the edge plasma provides an ionization particle ion source ($\nu_{\text{ion}j}^*$) and a charge-exchange and elastic scattering momentum sink ($M_{\theta j}$) for the main ion species. We have made a series of calculations, using the same basic model parameters as in the previous section, to investigate the effect of different concentrations of neutral particles in the plasma edge on the edge poloidal rotation. The results are shown in Fig. 3 for the medium collisionality case. As anticipated from the above physical considerations, an increasing concentration of neutrals in the plasma edge reduces the magnitude of the edge poloidal rotation of both ions and impurities and brings these two velocities closer together.

C. Effect of edge up-down asymmetry

A lower single null (LSN) or upper single null (USN) divertor configuration introduces an up–down asymmetry (ξ) into the flux surface geometry in the edge plasma. A series of calculations were made for USN and LSN configurations with the asymmetry factor varying over the range $0 \leqslant \xi/\epsilon \leqslant 1$. The results are shown in Fig. 4. The effect of edge up–down asymmetry is to reduce the magnitude of the edge poloidal rotation, and there is little difference between the USN and LSN configurations in this respect.

V. COMPARISON WITH OTHER NEOCLASSICAL POLOIDAL ROTATION MODELS

There are (at least) two other neoclassical models[12,13] in general use for the calculation of poloidal rotation, both based on the Hirsman–Sigmar (HS) fluid formulation of neoclassical thery,[14] as is the model of this paper and Ref. 4. In the HS fluid formalism, kinetic theory effects enter through the constitutive relations. In the constitutive relations used in

TABLE III. Variation of rotation with collisionality in a model with the parameters of DIII-D shot #98777 at 1600 ms. ($R=1.7$ m, $a=0.6$ m, $\kappa=1.7$, $|B_\phi|=1.6$ T, $I=1.2$ MA, $P_{\text{nbi}}=4.5$ MW.)

$\nu_D^{*\,a}$	$\nu_{\text{carb}}^{*\,a}$	$v_{\theta D}$ (m/s)[a]	$v_{\theta\text{carb}}$ (m/s)[a]	$v_{\phi 0}$ (m/s)	E_r (V/m)[a]	τ_ϕ^{th} (ms)
0.75	9.5	-0.38×10^3	-0.38×10^3	0.47×10^5	0.95×10^4	28
0.036	0.475	-0.43×10^3	-0.55×10^3	0.84×10^5	1.4×10^4	51
0.009	0.12	-0.68×10^3	-0.74×10^3	1.38×10^5	2.1×10^4	83
0.003	0.033	-1.19×10^3	-1.48×10^3	2.30×10^5	3.2×10^4	138
0.001	0.015	-1.72×10^3	-2.36×10^3	3.05×10^5	3.9×10^4	183
0.0004	0.006	-2.6×10^3	-4.29×10^3	4.65×10^5	5.6×10^4	279

[a]At $r/a=1/2$.

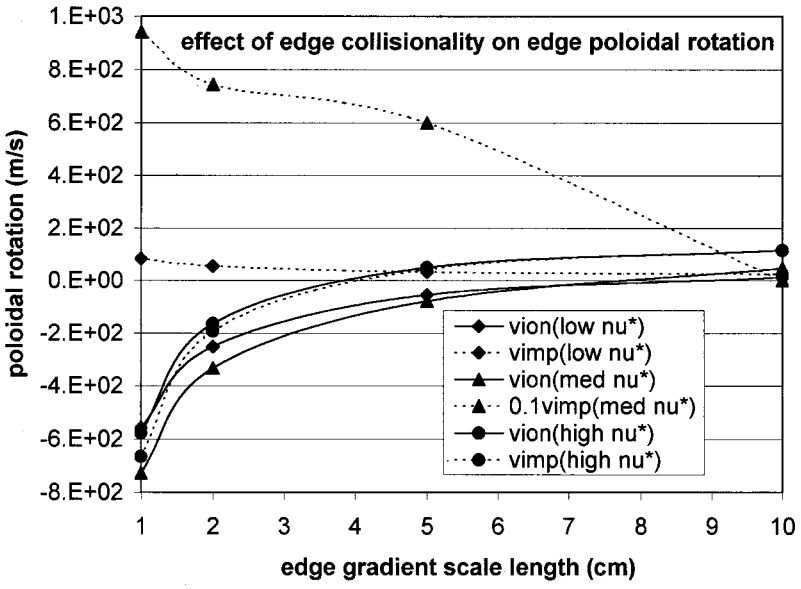

FIG. 2. Effect of edge pressure gradient and collisionality on edge poloidal rotation velocities for a model problem with parameters of DIII-D shot #98777 at 1600 ms. ($R=1.7$ m, $a=0.6$ m, $\kappa=1.7$, $|B_\phi|=1.6$ T, $I=1.2$ MA, $P_{\mathrm{nbi}}=4.5$ MW, $n_{\mathrm{edge}}=0.75\ \mathrm{m}^3$, $T_{\mathrm{edge}}=100$ eV, $v_{\phi\mathrm{edge}}=1.75\times10^4$ m/s, $n_{0\mathrm{edge}}=10^{15}\ \mathrm{m}^{-3}$, $\xi=0.0$.)

this paper and Ref. 4, the interspecies collisional friction is linearly related to the bulk flow velocities, and the parallel viscous force is linearly related to the bulk flow velocities and their gradients (with a viscosity coefficient due to Shaing[10]). References 12 and 13 use more complete constitutive expressions which relate the friction to both the bulk flow velocities and the bulk heat flows (with the HS friction coefficient[14]), and use expressions that relate the parallel viscous force linearly to bulk flow velocities and bulk heat flows and their gradients (using the HS viscosity coefficient[14] in Ref. 12 and using a later viscosity coefficient due to Shaing[15] in Ref. 13). The main effect of these differences in constitutive relationships is to introduce temperature gradient terms into the frictional and parallel viscous forces in Refs. 12 and 13 that are absent in this paper and Ref. 4. Inclusion of these bulk heat flow terms in the friction and parallel viscous forces of this paper, which we intend to do, would double the size of the coupled set of Eqs. (22)–(24), but this larger set of coupled equations presumably would still be solvable by the same general procedure. We note the existence of even more complete models for the parallel viscous force that include such effects as the poloidal variation of the viscous force,[16] orbit squeezing,[17] etc., which are not included in the poloidal rotation models of this paper and Ref. 4 or the models of Refs. 12 and 13.

Since in early neoclassical models[18] the poloidal rotation was proportional to the temperature gradient, it might be expected that the absence of the thermal friction force in the considerably more sophisticated model of this paper and Ref. 4 is a significant deficiency. It is not possible to check this directly. We can only note that the one calculation for an experiment presented in this paper was in agreement with the measured value to within the error bars. Quantitative evaluation of the effect of thermal friction on the calculation of poloidal rotation in the model of this paper must await future extension of this model.

On the other hand, there are two respects in which the model of this paper and Ref. 4 is more complete than the

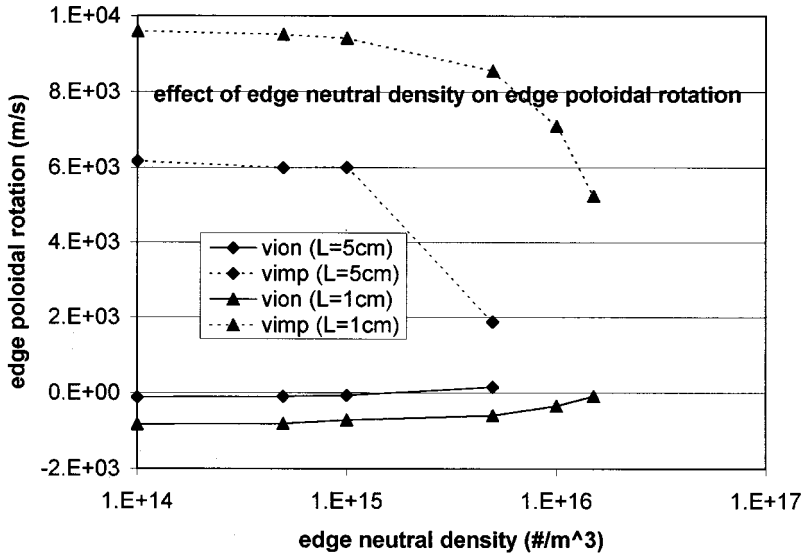

FIG. 3. Effect of edge neutral density on edge poloidal rotation velocities for a model problem with parameters of DIII-D shot #98777 at 1600 ms. ($R=1.7$ m, $a=0.6$ m, $\kappa=1.7$, $|B_\phi|=1.6$ T, $I=1.2$ MA, $P_{\mathrm{nbi}}=4.5$ MW, $n_{\mathrm{edge}}=0.75\ \mathrm{m}^{-3}$, $T_{\mathrm{edge}}=100$ eV, $v_{\phi\mathrm{edge}}=1.75\times10^4$ m/s, $\nu_D^*=0.14$, $\nu_{\mathrm{carb}}^*=1.78$, $\xi=0.0$.)

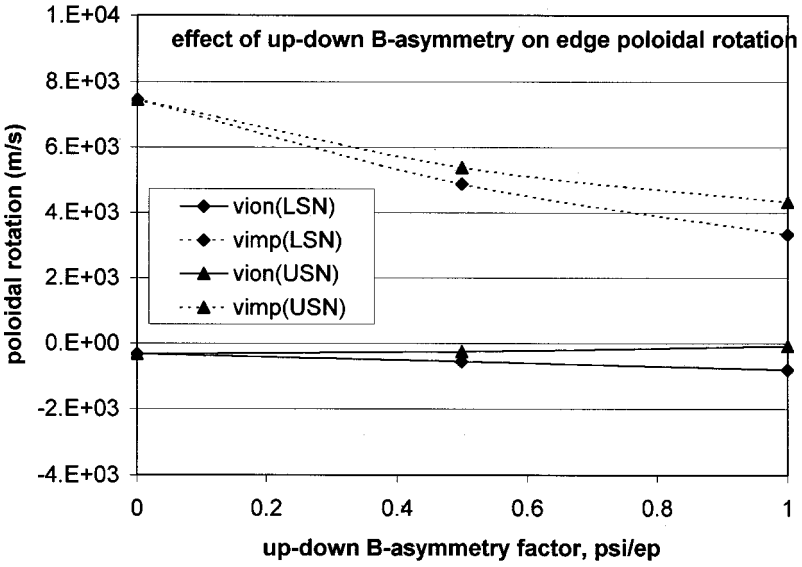

FIG. 4. Effect of edge up–down asymmetry on edge poloidal rotation velocities for a model problem with parameters of DIII-D shot #98777 at 1600 ms. ($R=1.7$ m, $a=0.6$ m, $\kappa=1.7$, $|B_\phi|=1.6$ T, $I=1.2$ MA, $P_{\rm nbi}=4.5$ MW, $n_{\rm edge}=0.75\,{\rm m}^{-3}$, $T_{\rm edge}=100$ eV, $v_{\phi{\rm edge}}=1.75\times10^4$ m/s, $n_{0{\rm edge}}=10^{15}\,{\rm m}^{-3}$, $\nu_D^*=0.14$, $\nu_{\rm carb}^*=1.78$.)

models of Refs. 12 and 13. These latter models only retain the first poloidal angular moment (the flux surface average) in developing the equations for the poloidal rotation velocities, while the model of this paper and Ref. 4 retains additional sine and cosine angular moments to derive coupled equations for the poloidal rotation velocities and poloidal density asymmetries. It is clear from Eq. (22) that the coupling to poloidal density asymmetries introduces important viscous and inertial driving and damping terms into the equations for the poloidal rotation velocity that could not arise in the models of Refs. 12 and 13. Furthermore, the poloidal and toroidal rotation velocities are coupled via a ''first principles'' neoclassical model for radial momentum transport in this paper (Sec. II N) and Ref. 4, while an *ad hoc* ''anomalous'' radial momentum transport term must be input to couple the calculation of poloidal and toroidal rotation velocities in the models of Refs. 12 and 13.

It also appears that force terms arising from electric fields, beam momentum input and inertial effects are missing in the model of Ref. 12.

VI. SUMMARY

We have refined and extended our original neoclassical calculation model for the poloidal velocities and poloidal density asymmetries in a multi-species tokamak plasma. The refinements make more explicit in the formalism the directions of the current, magnetic field and beam momentum input, and introduce a more rigorous representation of the poloidal variation of the toroidal rotation velocity, which is needed as an input to the calculation of poloidal rotation and poloidal density asymmetries. The introduction of new terms representing pressure gradients, ionization particle sources, charge-exchange momentum sinks, and up–down flux surface asymmetries extends the applicability of the calculation model to the edge plasma.

The refined model for the calculation of poloidal rotation and density asymmetries in the core plasma was combined with a neoclassical gyroviscous momentum transport model and a toroidal rotation calculation model. The combined model was used to calculate toroidal and poloidal rotation velocities, momentum confinement times and radial electric fields in good agreement with measurements in a DIII-D shot and to investigate the predicted directionality and collisionality dependencies of these quantities.

We have performed a series of calculations to investigate the effects of pressure gradient, neutral density, and up–down asymmetry on poloidal rotation in the edge plasma. We find that increasing the steepness of the edge pressure gradient increases the magnitude of the edge poloidal rotation velocities, while increasing the edge neutral density or the edge up–down asymmetry factor reduces the magnitude of the poloidal rotation in the plasma edge. The edge collisionality was found to have important effects on the edge poloidal rotation.

To put this paper in perspective, we reiterate that although the refined and extended model for the calculation of poloidal rotation and poloidal density asymmetries presented herein could be used in a ''stand-alone'' mode if the toroidal rotation is treated as a known input quantity, this model is intended as part of a coupled neoclassical model[4] for the calculation of poloidal and toroidal rotation that requires only the beam momentum (and the plasma density and temperature) as input.

[1]W. M. Stacey, Phys. Fluids B **4**, 3302 (1992).
[2]W. M. Stacey and D. J. Sigmar, Phys. Fluids **28**, 2800 (1985).
[3]W. M. Stacey and D. R. Jackson, Phys. Fluids B **5**, 1828 (1993).
[4]W. M. Stacey, Phys. Plasmas **8**, 158 (2001).
[5]W. M. Stacey and M. Murakami, Phys. Plasmas **8**, 4450 (2001).
[6]W. M. Stacey and J. Mandrekas, Phys. Plasmas **9**, 1622 (2002).
[7]R. J. Groebner, K. H. Burrell, and R. P. Seraydarian, Phys. Rev. Lett. **64**, 3015 (1990).
[8]E. J. Doyle, R. J. Groebner, K. H. Burrell *et al.*, Phys. Fluids B **3**, 2300 (1991).
[9]R. J. Groebner, Phys. Fluids B **5**, 2343 (1993).
[10]W. M. Stacey, A. W. Bailey, D. J. Sigmar, and K. C. Shaing, Nucl. Fusion **25**, 463 (1985).
[11]K. H. Burrell, General Atomics, personal communication (2001).

[12]Y. B. Kim, P. H. Diamond, and R. J. Groebner, Phys. Fluids B **3**, 2050 (1991).
[13]W. A. Houlberg, K. C. Shaing, S. P. Hirshman, and M. C. Zarnstorff, Phys. Plasmas **4**, 3230 (1997).
[14]S. P. Hirshman and D. J. Sigmar, Nucl. Fusion **21**, 1079 (1981).
[15]K. C. Shaing, M. Yokoyama, M. Wakatoni, and C. T. Hsu, Phys. Plasmas **3**, 965 (1996).
[16]J. P. Wang and J. D. Callen, Phys. Fluids B **5**, 3207 (1993).
[17]K. C. Shaing and R. D. Hazeltime, Phys. Plasmas **1**, 3365 (1994).
[18]R. D. Hazeltime, Phys. Fluids **17**, 961 (1974).